EPJ manuscript No.
(will be inserted by the editor)

The ^{3}He+^{5}He$\rightarrow \alpha$+α reaction below the Coulomb barrier via the Trojan Horse Method

C. Spitaleri[1,2a], S. Typel[3,4], C.A. Bertulani[5], A.M. Mukhamedzhanov[6], T. Kajino[7,8,9], M. Lattuada[1,2], A. Cvetinović[10], S. Messina[1], G.L. Guardo[1], N. Soić[11], M. Milin[12], S.S. Perrotta[1,2,13], Chengbo Li[14], P. Čolović[11], G. D'Agata[15], D. Dell'Aquila[11], C.G. Fatuzzo[16], M.Gulino[1,17], S.Q. Hou[18], M. La Cognata[1], D. Lattuada[1,17], D. Nurkić[12], R. Popočovski[11], N. Skukan[11], S. Szilner[11], O. Trippella[19], M. Uroić[11] and N. Vukman[11].

[1] INFN - Laboratori Nazionali del Sud, via S. Sofia 62, 95123 Catania, Italy,
[2] Dipartimento di Fisica e Astronomia "Ettore Majorana", Universitá degli Studi di Catania, Catania, Italy
[3] Technische Universität Darmstadt, Fachbereich Physik, Institut für Kernphysik, Darmstadt, Germany
[4] GSI Helmholtzzentrum für Schwerionenforschung GmbH, Darmstadt, Germany
[5] Department of Physics and Astronomy, Texas A&M University-Commerce, Commerce, TX 75429, USA
[6] Cyclotron Institute, Texas A&M University, College Station, Texas, US
[7] National Astronomical Observatory of Japan, Mitaka, Tokyo 181-8588, Japan
[8] Graduate School of Science, The University of Tokyo, Bunkyo-ku, Tokyo 113-0033, Japan
[9] School of Physics, Beihang University, Beijing 100083, People's Republic of China
[10] Jožef Stefan Institute, Ljubljana, Slovenia
[11] Ruder Bošković Institute, Zagreb, Croatia
[12] Department of Physics, Faculty of Science, University of Zagreb, Zagreb, Croatia
[13] Departamento de Física Atómica, Molecular y Nuclear, Universidad de Sevilla, Siviglia, Spain
[14] Beijing Radiation Center, Beijing Academic of Science and Technology, Beijing, China
[15] Department of Nuclear Reactions, Nuclear Physics Institute of CAS, Prague, Czech Republic
[16] Materials Science Division, Lawrence Berkeley National Laboratory, Berkeley, California 94702, USA
[17] Facoltá di Ingegneria e Architettura, Universitá degli Studi di Enna "Kore", Enna, Italy
[18] Key Laboratory of High Precision Nuclear Spectroscopy, Institute of Modern Physics, Chinese Academy of Sciences, Lanzhou, China
[19] INFN Sezione di Perugia, Perugia, Italy

Received: date / Revised version: date

Abstract. For the first time in an application to nuclear astrophysics, a process induced by the unstable ^{5}He = (^{4}He-n) nucleus, the ^{3}He+^{5}He$\rightarrow 2\alpha$ reaction, has been studied through the Trojan Horse Method (THM). For that purpose, the quasi-free (QF) contribution of the ^{9}Be(^{3}He,$\alpha\alpha$)^{4}He reaction was selected at $E_{^3\mathrm{He}} = 4$ MeV incident energy. The reaction was studied in a kinematically complete experiment following a recent publication [1], where for the quasi free contribution the momentum distribution between α and ^{5}He particle cluster in the ^{9}Be nucleus in the ground state have been extracted. The angular distribution of the QF ^{3}He+^{5}He$\rightarrow 2\alpha$ reaction was measured at $\theta_{cm} = 78^\circ - 115^\circ$. The energy dependence of the differential cross section of the ^{3}He+^{5}He$\rightarrow 2\alpha$ virtual reaction was extracted in the energy range $E_{cm} = 0 - 650$ keV. The total cross section obtained from the Trojan-horse method was normalized to absolute cross sections from a theoretical calculation in the energy range $E_{cm} = 300 - 620$ keV.

PACS. PACS-key Nuclear Structure and Reactions – PACS-key Nuclear Astrophysics

1 Introduction

The investigation of nuclear reactions induced by an unbound nucleus x_{unb} is important for nuclear physics in the future. It could also be of interest to nuclear astrophysics if applied to reactions induced on unstable nuclei. At present, the direct investigation of a x_{unb}+B nuclear reaction (with x_{unb} as target or projectile) is not feasible, the most viable method to experimentally study the two-body reaction $x_{unb} + B \rightarrow C + D$ is to measure the inverse reaction. An alternative way to increase the possibility of measuring the cross sections of this type of nuclear reactions is to apply indirect methods. Those methods have been developed in the last decades mainly for astrophysical purpose, aiming to study nuclear reactions at very low

[a] *e-mail:* spitaleri@lns.infn.it

energies. Among these the Trojan Horse method (THM) [2–14] can be considered as an attractive way to evaluate the bare nucleus cross sections of rearrangement reactions induced by unstable nuclei [15–18]. In this approach, the reaction A+B → S+C+D with a spectator nucleus S is investigated instead of the reaction x_{unb}+B → C+D (see the upper panel in Fig. 1). In particular, in a previous experiment [17], the THM has already been applied to investigate the ^{8}Be(d,α)^{6}Li reaction, induced by the unbound nucleus ^{8}Be, at energies of astrophysical interest by studying the quasi-free (QF) contribution to the ^{2}H(^{9}Be,α^6Li)n reaction.

In the present work, the THM was used to extract the cross section of the ^{3}He(^{5}He,α)^{4}He reaction, by measuring the QF contribution of the ^{9}Be(^{3}He,$\alpha\alpha$)^{4}He reaction. A preliminary study of the reaction mechanisms involved in the ^{3}He(^{9}Be,$\alpha\alpha$)^{4}He reaction has already been carried out, by testing the presence of the QF contribution at energies compatible with the particular kinematic conditions suitable for the application of the THM [1]. Furthermore, the ^{5}He-^{4}He inter-cluster momentum distribution in the ^{9}Be nucleus was measured with different analysis methods. These preliminary investigations are the necessary conditions to study of the ^{5}He(^{3}He,α)^{4}He virtual reaction by applying the THM (see Ref. [1]).

Moreover, the ^{9}Be(^{3}He,$\alpha\alpha$)^{4}He reaction at beam energies comparable to the height of the Coulomb barrier was experimentally investigated by several authors showing a clear evidence of a QF contribution at low incident energies [19–23] (see Table 1). In particular, the α-α coincidence cross section for the ^{9}Be(^{3}He,$\alpha\alpha$)^{4}He reaction at 4 MeV of the beam energy has been measured showing that under some specific kinematic conditions the primary reaction mechanism was a direct interaction between the ^{3}He projectile and the ^{5}He cluster in the target [19]. In this case, as shown in Fig. 1b, the two α-particles are emerged after the QF pickup reaction, while the other cluster, again an α-particle, acts as a spectator to the process (α_S).

To verify whether the contribution of the QF mechanism was present in the low-energy range, the ^{9}Be(^{3}He,$\alpha\alpha$)^{4}He reaction was studied at different energies (2.5, 2.7 and 2.8 MeV) [20,24]. Moreover, the excitation function of the three-body cross section has been measured both at symmetrical and asymmetrical detection geometries[19,20,24].

In a past experiment [21], the Treiman-Yang criterion [25] was also applied to the ^{9}Be(^{3}He,$\alpha\alpha$)^{4}He reaction, offering further evidence for the validity of the pole approximation in the present case.

The aim of the present work is to determine the excitation function and angular distributions of the ^{5}He(^{3}He,α)^{4}He reaction at low energies in the center of mass system ($0 \leq E_{c.m.} \leq 620$ keV).

2 Basic features of the Quasi Free reaction mechanism

Before proceeding with the experimental details of the present study, a brief presentation of the basic theory behind the QF mechanism is given here, primary to provide a better understanding of the reaction mechanisms that are involved in the ^{9}Be(^{3}He,$\alpha\alpha$)^{4}He reaction at low energies.

Table 1. Results of previous works on the ^{9}Be(^{3}He,$\alpha\alpha$)^{4}He reaction (Q-value = 19.005 MeV). The beam energy (E_{beam}), corresponding energy in the center-of-mass system (E_{cm}), transferred momentum (q_t), de Broglie wavelength (λ), publication year and reference are given for each measurement. The binding energies for the ^{9}Be and ^{5}He in ground state are are 2.46 MeV and −0.89 MeV respectively.

E_{beam} (MeV)	E_{cm} (MeV)	q_t (MeV/c)	λ (fm)	Year	Ref
2.5	1.8	420	1.67	1978	[23]
2.7	2.0	420	1.61	1978	[23]
2.8	2.1	421	1.58	1979	[20]
3.0	2.3	425	1.52	1986	[22]
4.0	3.0	430	1.32	1975	[19]
4.0	3.0	430	1.32	2019	[14]
12	9.0	485	0.76	1986	[22]

The theory of direct reactions is the background for the study of QF processes [26,27]. The QF mechanism is already well known as typical mechanism present in nuclear reactions at high energies where the average Galilean-invariant momentum q_t [28] transferred to the detected α particles is of the order of hundreds MeV/c, so the conditions of the Impulse Approximation (IA) is well fulfilled [28,29]. Moreover, a high projectile energy implies a small de Broglie wavelength and, consequently, allows the projectile to "*see*" only one cluster and interact with it with a negligible influence from the remaining part of the target nucleon. The de Broglie wavelengths $\lambda = \hbar/p$, where p is the momentum of the projectile calculated for different beam energies, see Table 1, are significantly smaller than the inter-cluster distance confirming that the 4 MeV ^{3}He beam provides a good probe of the THM mechanism described by the simple diagram shown in Fig. 1a [30,31].

The study of the QF process is often performed in the framework of the Plane Wave Impulse Approximation (PWIA) or the Distorted Wave Impulse Approximation (DWIA), without spin-orbit dependent distortions. Under these conditions, the three-body reaction cross section is proportional to the cross section of the virtual two-body reaction:

$$\frac{d^3\sigma}{d\Omega_{\alpha_1} d\Omega_{\alpha_2} dE_{\alpha_1}} \propto (KF) \cdot |\phi(p_{\alpha_S})|^2 \cdot \left[\frac{d\sigma}{d\Omega}\right]^{HOES}_{^3He+^5He\rightarrow\alpha+\alpha} \quad (1)$$

where:

1. $\left[\frac{d\sigma}{d\Omega}\right]^{HOES}_{^3He+^5He\rightarrow\alpha+\alpha}$ is the half-off-energy-shell (HOES) differential cross section for the virtual ^{3}He+^{5}He→

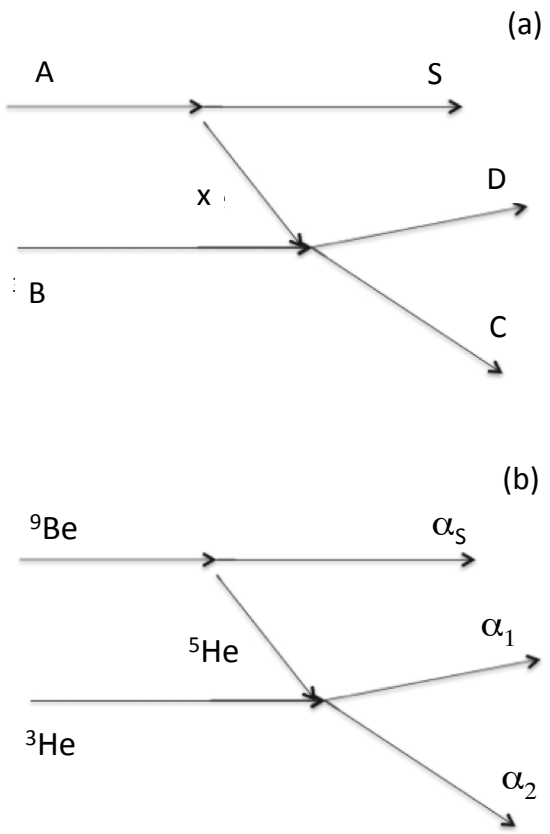

Fig. 1. Diagram describing the QF process for generic A+B→ C+D+S three body reaction is given in upper panel, while for the measured ^{9}Be(^{3}He,$\alpha\alpha$)^{4}He reaction is given in lower panel. Particle x (^{5}He) is called "participant" to the process while S particle is called "spectator" (α_S) to the B+$x \rightarrow C$+D (^{5}He+^{3}He $\rightarrow \alpha_1 + \alpha_2$) virtual reaction.

α_1+α_2 two body reaction at center of mass energy E_{cm}. It can be expressed with the Post Form Prescription (PFP) as [32]:

$$E_{cm} = E_{\alpha_1\alpha_2} - Q_{2b} \quad (2)$$

where Q_{2b} is the Q-value of the ^{3}He+^{5}He→ α_1+α_2 binary reaction and $E_{\alpha_1\alpha_2}$ is the $\alpha_1 - \alpha_2$ relative energy in the exit channel.

2. KF is a kinematic factor containing the final state phase space factor. It depends on masses, momenta and angles of the detected particles [19].
3. $|\phi(p_{\alpha_S})|^2$ is the momentum distribution of the spectator α_S. It is given in PWIA by the square of the Fourier transform of the radial inter-cluster wave function. Since the dominant configuration of the ^{4}He-^{5}He partition in ^{9}Be is characterized by l=0, $|\phi(p_{\alpha_S})|^2$ is centered at $|\boldsymbol{p}_{\alpha_S}|$=0 [22,33,34]. Any contribution from higher angular momenta l will correspond to a momentum distribution that peaks at finite values of p_{α_S}. In the selected low-momentum momentum range for the analysis it can be neglected as compared to the dominant $l = 0$ component considering the uncertainties.

The region where the pole diagram (Fig. 1) is expected to be dominant is fixed by the condition [31]:

$$0 \leq p_{\alpha_S} \leq \kappa \quad (3)$$

where κ_{xS} is the wave number of bound state (xS)

$$\kappa_{xS} = \sqrt{2\mu_{(xS)}B_{(xS)}} \quad (4)$$

where $\mu_{(xS)}$ and $B_{(xS)}$ are the reduced mass and the binding energy of the xS (^{5}He-^{4}He) cluster system in the A (^{9}Be) nucleus with respect to the breakup into ^{4}He and ^{5}He, respectively (Fig. 1).

The validity conditions of the IA have been checked for the ^{9}Be(^{3}He,$\alpha\alpha$)^{4}He reaction. Indeed, the Galilean invariant transferred momentum q_t is 430 MeV/c (for the 4 MeV beam energy) with an associated de Broglie wavelength of $\lambda\!\!\!^{-} = 1.32$ fm. This has to be compared with the ^{9}Be nucleus radius which is around 5 fm [24,28,29]. Furthermore, as a pole approximation validity test, the Treiman-Yang (T-Y) criterion [25,35] has been successfully applied to the ^{9}Be(^{3}He,$\alpha\alpha$)^{4}He reaction at 2.8 MeV energy beam [21]. The T-Y test, which has the advantage of being based only on general principles of physics, regardless of nuclear reaction models, has provided further confidence on the validity of the pole approximation and therefore of the factorization applied (Eq.(1)) to the three-body cross section of interest [21]. The theoretical details of the T-Y criterion are briefly provided in section 5 of this work.

3 Experimental setup

The experiment was performed using the EN Tandem at the Ruder Boskovíc Institute in Zagreb. A ^{3}He beam with an energy of 4 MeV and with intensity of $7 - 10$ nA was delivered onto a ^{9}Be target, $\sim$ 124 μg/cm^2 thick, evaporated on a thin carbon foil, $\sim$ 40 μg/cm^2 thick, placed at 90° with respect the beam direction. The beam energy has been chosen in order to maximize the QF contribution [22]. In addition, at this beam energy two experimental data sets are available in the literature (as reported in Table 1), useful for a data comparison and normalization [19,22].

The experimental setup consisted of four single-sided silicon Position Sensitive Detectors (PSD), two 1000 μm and two 500 μm thick, mounted in a co-planar geometry on both sides of the beam direction covering a solid angle of 3.5 msr. A sketch of the adopted setup is depicted in Fig. 2. The α-α coincidences were measured by any pair of PSD's placed on opposite sides of the beam direction. A detailed description of the experimental setup with positions, distances, solid angles and other characteristics of the used detectors can be found in ref [14]. No particle identification technique was used during the experiment, since the Q-value (19.9 MeV) of the three-body reaction of interest is the largest among the other possible three-body reactions occurring on carbon, oxygen and other elements present in the target.

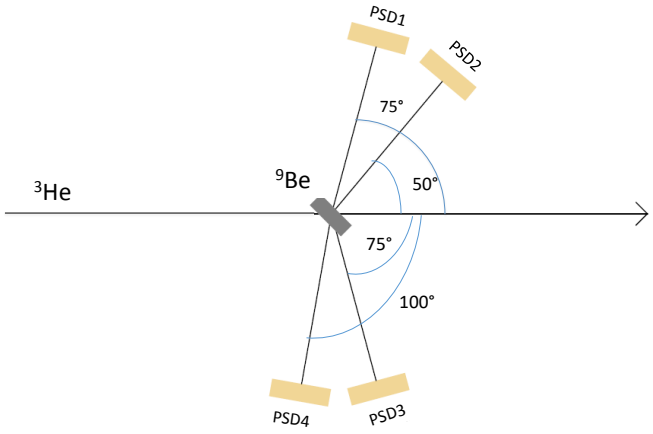

Fig. 2. Schematic drawing of the experimental setup adopted for the study of the ^{9}Be(^{3}He,$\alpha\alpha$)^{4}He reaction.

The energy calibration was performed using elastic and inelastic scattering of the ^{3}He at 4 MeV on a ^{197}Au target. Moreover, a three-peak α source (^{239}Pu (5.157 MeV), ^{241}Am (5.486 MeV) and ^{244}Cm (5.805 MeV)) was employed. The position calibration was performed using a grid with 18 equally spaced slits in front of each detector. An overall energy resolution of about 1% and angular resolution of $0.3° - 0.5°$ was obtained. The beam spot size ($\sim$ 1.5 mm) and energy spread were taken into account, as well as the energy loss in the target and in the dead layers of the detectors.

4 Data analysis

The extraction of the ^{3}He+^{5}He $\rightarrow 2\alpha$ two-body cross section via the THM follows a standard data analysis path that can be summarized as follow:

1: Selection of the best suitable Trojan Horse nucleus;
2: Selection of the ^{9}Be(^{3}He,$\alpha\alpha$)^{4}He three-body channel;
3: Selection of the events from the QF reaction mechanism;
4: Validity tests of the selected data;
5: Evaluation of the differential three body cross section;
6: Extraction of the angular distribution of two-body virtual $d\sigma(E_{cm})^{HOES}/d\Omega$ cross section;
7: Integration and normalization of data for the extraction of the two body cross section of interest in absolute units.

These steps will be described in the following sections.

4.1 Selection of the Trojan Horse nucleus

Table 2 shows the main TH-nuclei used as sources of virtual targets or projectiles in the past applications of the THM. It is useful here to briefly recall that in the general case of a reaction $A(B,CD)S$, the nucleus A is called a "Trojan Horse nucleus" for the investigation of the x+B→C + D virtual reaction if it can be described by a cluster structure ($x + S$)

Among the other TH-nuclei, it should be noted that the ^{9}Be nucleus represents an interesting candidate thanks to its pronounced cluster configurations (^{8}Be-n and ^{5}He-^{4}He) [14]. This implies that it can be used as virtual source of α, ^{5}He, ^{8}Be, or n. Therefore the ^{9}Be nucleus can be considered as TH-nucleus for reactions induced by unstable nuclei like ^{5}He (present work) or ^{8}Be [17].

4.2 Selection of the ^{9}Be(^{3}He,$\alpha\alpha$)^{4}He three-body channel

It is well known that in a reaction with three particles in the exit channel, two-dimensional plots between the energies of any two of the emitted particles show their correlation in terms of energy and momentum conservation. Thus, they can be used to select the reaction channel of interest. In our case, only two of the three emitted particles were detected, leaving, in general, the system undetermined due to the overlapping of different kinematic loci in the same phase-space region. Those loci correspond to reactions of the ^{3}He beam with nuclei that constitute impurities in the targets, producing different undetected particles. Thus, the aforementioned procedure should not introduce ambiguities in the present case, due to the high Q-value (19.004 MeV) of the reaction of interest, much larger for than any other possible reaction occurring on carbon backing or impurities in the target.

Nonetheless, to avoid errors introduced by unknown impurities in the target or beam, a further check based on the mass identification [36] of the undetected spectator particle S was carried out. The applied procedure is given in more details in [1]. Taking into account the energy and momentum conservation laws and by considering an undetected particle having mass number 4, the experimental Q-value spectrum for the selected events was reconstructed: the corresponding spectrum of events in detectors PSD1 and PSD3 is shown in Fig. 3. This spectrum shows a prominent peak at ∼19 MeV in good agreement with the expected Q-value of 19.004 MeV (marked by an arrow in Fig. 3). No evidence of contamination events is present in the Q-value spectrum. Only events inside the limits 18.75 MeV≤ (Q-value)≤19.2 MeV were selected for the subsequent data analysis.

A demonstration of the good channel selection is given in Fig. 4, where the experimental kinematic locus for two coincident α_1 and α_2 detections is reported for a chosen angular pair, namely $\theta_{PSD_1} = |\theta_{PSD_3}| = 75° \pm 1°$. Here, the energy detected in PSD_1 is given on the horizontal axis, while the energy deposited in PSD_3 is indicated on the vertical axis. Experimental data are clearly distributed along an ellipse, owing to events from the ^{9}Be+^{3}He reaction. The experimental locus is compared with a simulated two-dimensional spectrum (red points), which accounts for the energy loss and the experimental and kinematic constraints. Good agreement between the experimental and

Table 2. The TH-nuclei used in the past for application of THM. Here we report the cluster structures, the relative binding energies, the used virtual particles and the application for specific reactions with the corresponding references. It is important to underline that the ^{9}Be nucleus represents an interesting candidate to be used as "Trojan Horse nucleus" for its versatile configuration.

Nucleus "TH"	Main cluster structure	Binding energy (MeV)	Virtual particle transferred	2-body reaction	3-body reaction	Ref
d	p-n	2.2	p	^{7}Li(p,α)^{4}He	^{7}Li(d,2α)n	[37–39]
^{3}He	p-d	5.5	p	^{7}Li(p,α)^{4}He	^{7}Li(^{3}He,2α)^{2}H	[40]
^{6}Li	α-d	1.5	d	^{2}H(^{6}Li,α)^{4}He	^{6}Li(^{6}Li,α α)^{4}He	[4,41,42]
^{3}He	p-d	5.5	d	^{2}H(^{6}Li,α)^{4}He	^{6}Li(^{3}He,α α)^{1}H	[42]
^{6}Li	α-d	1.5	d	^{2}H(d,^{3}He)n	^{2}H(^{6}Li,^{3}He n)^{4}He	[43]
^{3}He	d-p	5.5	d	^{2}H(d,^{3}He)n	^{2}H(^{3}He,^{3}He n)^{1}H	[44]
^{6}Li	α-d	1.5	d	^{2}H(d,^{3}H)^{1}H	^{2}H(^{6}Li,^{3}H p)^{4}He	[45]
^{3}He	d-p	5.5	d	^{2}H(d,^{3}H)^{1}H	^{2}H(^{3}He,^{3}He n)^{1}H	[44,45]
^{6}Li	α-d	1.5	α	^{13}C(α,n)^{16}O	^{13}C(^{6}Li,n^{16}O)^{2}H	[46]
d	p-n	2.2	n	^{17}O(n,α)^{14}C	d(^{17}O,α^{14}C)p	[47]
^{9}Be	n-^{8}Be	2.5	^{8}Be	^{8}Be(d,α) ^{6}Li	^{9}Be(d,α ^{6}Li)n	[17]
^{9}Be	α-^{5}He	2.5	^{5}He	^{5}He(^{3}He,α)^{4}He	^{9}Be(^{3}He,$\alpha\alpha$)^{4}He	[pres. work].

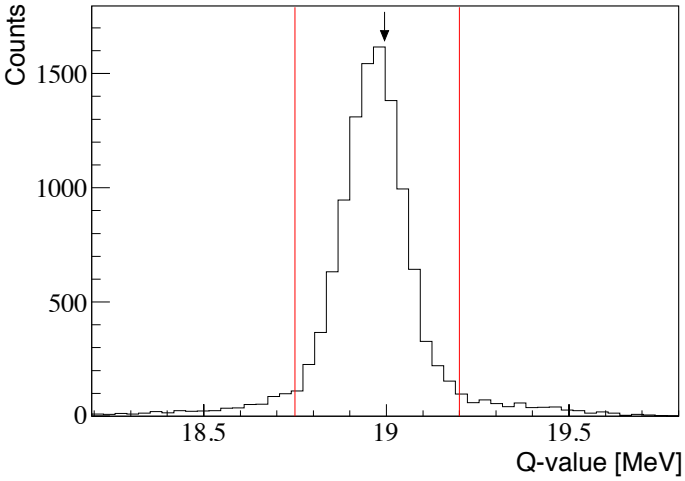

Fig. 3. Q-value spectrum obtained for coincidence events in the detectors PSD$_1$ and PSD$_3$. The sharp peak around 19 MeV contains only the ^{9}Be(^{3}He,$\alpha\alpha$)^{4}He events. The arrow indicates the energy corresponding to the theoretical Q-value. In the data analysis only the events between the two red lines were taken into consideration. The background of the data that cannot be associated with the ^{9}Be(^{3}He,$\alpha\alpha$)^{4}He reaction is negligible (∼3%). The uncertainty associated with it is taken into account in the calculation of the total uncertainties.

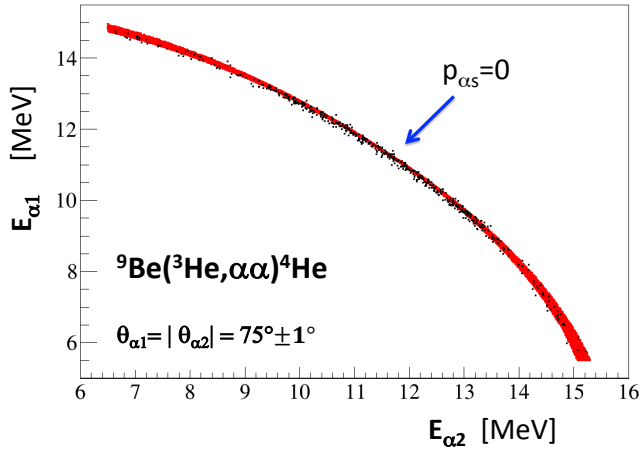

Fig. 4. Example of two dimensional E_{α_1}-E_{α_2} energy spectrum. E_{α_1} and E_{α_2} stand for the energies of the particles measured in the detectors PSD$_1$ and PSD$_3$, respectively. The experimental kinematic locus E_{α_1}-E_{α_2} (black points) at symmetric quasi-free angles $\theta_1 = |\theta_2| \sim 75° \pm 1°$ is depicted indicating a good agreement with the simulated one (red points). The arrow marks the region where $E_{\alpha_1} = E_{\alpha_2}$ and p_{α_S}=0

simulated kinematic loci is found for all the angular couples, strongly confirming the good selection of the three-body channel of interest.

In Fig. 4, the condition of $p_{\alpha_S} = 0$ (or E_{α_S}=0) corresponds to a point with $E_{\alpha_1} = E_{\alpha_2}$, since the two particles are identical and detected at symmetric angles (at beam energy of 4 MeV with $E_{\alpha_1} = E_{\alpha_2} \sim 11.6$ MeV).

In the following, the detected α particles from any of the selected coincidences will be indicated with symbols α_1 (particle detected in PSD1) and α_2 (particle detected in PSD3), while α_S will stand for the undetected α particle.

4.3 Selection of events from the QF reaction mechanism

The next step in a TH analysis is the identification of different reaction mechanisms with the same three α in the final state. Indeed, for the application of the THM only the QF events should be selected. In general, the selection

of events related to the QF mechanism is complicated by the presence of other reaction mechanisms producing the same three particles in the final state (Fig. 5), namely the sequential decay (SD) (Fig. 5(a)) and direct breakup (DB) (Fig. 5(b)).

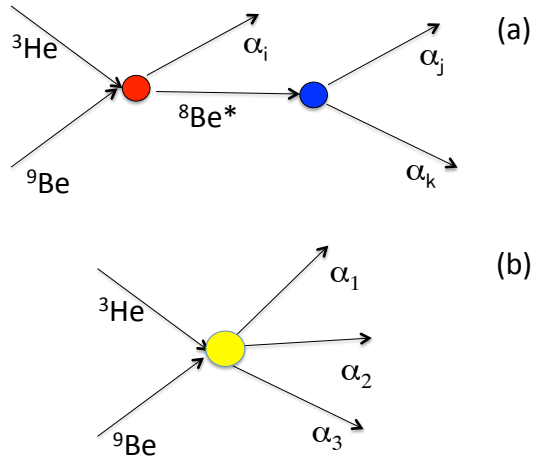

Fig. 5. Simplified diagrams for the main reaction mechanisms different to the QF one (Fig. 1) in the three-body nuclear reactions. Diagram (a) represents a two step process proceeding through the sequential decay (SD) of an intermediate ^{8}Be level. Diagram (b) represents a direct 3-α breakup mechanism (DB).

A standard way to investigate the reaction mechanisms is the study of the experimental momentum distribution $|\phi(\boldsymbol{p}_{\alpha_S})|^2_{exp}$ [14,48]. Indeed, the shape of the experimental momentum distribution of the inter-cluster motion of ^{5}He inside ^{9}Be is very sensitive to the reaction mechanism, so its extraction and comparison with theoretical models is a necessary test to confirm the applicability of the THM [1].
For this purpose, according to the available data, this work was preceded by the study of the QF reaction mechanism and the related momentum distributions were measured through different methods.

The experimental momentum distribution can be calculated via the formula:

$$|\phi(\boldsymbol{p}_{\alpha_S})|^2_{exp} \propto \frac{Yield}{(KF)\cdot\left[(\frac{d\sigma}{d\Omega})^{HOES}\right]_{^5He(^3He,\alpha)^4He}} \quad (5)$$

where the kinematic factor (KF) takes into account the angles ($\theta_{\alpha_1}$and θ_{α_2}) and energies ($E_{\alpha_1}$and E_{α_2}) of the detected α_1 and α_2 particles (Eq. (1)).
For particular kinematic conditions of the angular ($\Delta\theta_{cm}$) and energy ranges (ΔE$_{cm}$), the differential cross section

$$\left[\frac{d^2\sigma(\Delta\theta_{cm},\Delta E_{cm})}{d\Omega dE})\right]^{HOES} \quad (6)$$

can be considered constant.

The momentum distribution $|\phi(\boldsymbol{p}_{\alpha_S})|^2_{exp}$ can be described by the modulus square of the momentum-space wave function of the ^{4}He-^{5}He relative motion. It is obtained from the coordinate-space wave function by a Fourier transform. Assuming a spherical Hankel function with $l = 0$ and imaginary argument $i\kappa_{xS}r$ as the radial wave function for radii r larger than a cut-off radius R and zero for $r < R$, we find

$$|\phi(\boldsymbol{p}_{\alpha_S})|^2_{exp} = \frac{N}{(k^2_{\alpha_S}+\kappa^2_{xS})^2}\left[\frac{\sin(k_{\alpha_S}R)}{k_{\alpha_S}}+\frac{\cos(k_{\alpha_S}R)}{\kappa_{xS}}\right]^2 \quad (7)$$

with a normalization constant N, $k_{\alpha_S} = p_{\alpha_S}/\hbar$ and the bound-state wave number κ_{xS} defined in Eq. (4). This form gives a very good approximation to the momentum distribution of a more realistic wave function with a Whittaker function for the correct asymptotic radial dependence.

Fig. 6 shows the fit (red line) of the average experimental impulse distribution while the dashed blue lines represent the upper and lower ends of the fit, taking into account the uncertainties on the measurements of the impulse distributions. The procedure adopted to select the QF events from the experimental data is explained in detail in [1]. The conclusions drawn in [1] make us confident that a good selection of the QF mechanism in the analyzed data was achieved.

4.4 Selection of the events for the ^{5}He(^{3}He,α)^{4}He investigation

After the selection of the events from the ^{9}Be+^{3}He→3α reaction channel, the next step is to examine if, in the considered QF kinematic region, the contribution of the QF process to the overall α-α coincidence yield was evident and well separated from the other channels (Fig.5).

The upper part of Fig. 7 shows the simulated kinematic locus corresponding to the expected α_1-α_2 correlations, the red line indicates the energy of the level (1) reported in the literature (see parameters level (1) in Table 3). The intersection identifies the region in which the possible populated levels could make a contribution that would constitute a background for the data of interest.

In the lower part of the Fig. 7 the experimental coincidence yield for the α_1-α_2 particles is reported (black points). The arrows indicate the energy position of the sequential contributions through the ^{8}Be excited states (as reported in Table 3). The figure shows possible contributions from the unresolved levels at energies of 16.6 MeV and 16.9 MeV (labeled as (3) and (4) in Table 3), from unresolved levels at 19.2 MeV and 19.8 MeV (labeled as (5) and (6) in Table 3) and (7) + (8) from the unresolved levels at 20.1 MeV and 20.2 MeV (labeled as (7) and (8) in Table 3) while the label (1) refers to the level at 3.03 MeV in ^{8}Be. The contribution from level (2) is not visible due to its large width of about 3.5 MeV.

The red points in the lower part of Fig. 7 refer to the the coincidence yield corresponding to the $|\boldsymbol{p}_{\boldsymbol{\alpha_S}}| \leq$ 40 MeV/c momentum range. This selection allow us to

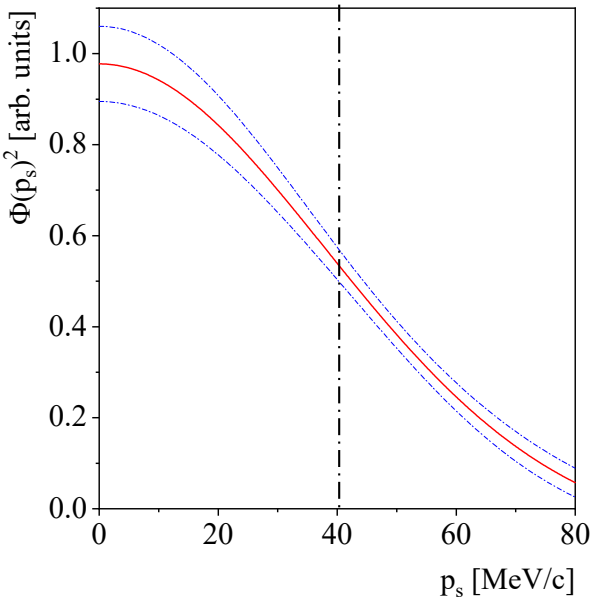

Fig. 6. Experimental momentum distribution as obtained in [14]. Fit of extracted average experimental impulse distribution obtained by four different experimental distributions measured with different methods: energy sharing ($\epsilon = 10\%$), angular correlation ($\frac{\Delta FWHM}{FWHM} = \epsilon = 8.1\%$), relative energy cut ($\epsilon = 9.8\%$), momentum bins ($\epsilon = 9.5\%$) reported in Ref. [1]. The best fit curve is shown as a red solid line, having $R_c = 4.9 \pm 0.3$ fm, a corresponding (FWHM)= (∼)82 ± 8 MeV/c and reduced χ^2 equal to ∼ 2.4. The blue dotted lines mark the $\pm 1\sigma$ confident bands of the fit.

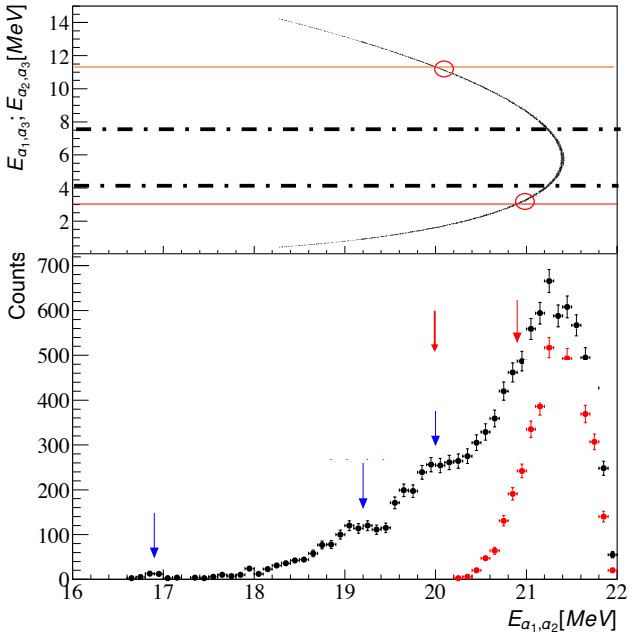

Fig. 7. Upper panel: Simulated $E_{\alpha_1\alpha_2}$, $E_{\alpha_1\alpha_S}$ correlation plot for symmetrical QF angles $|\theta_{\alpha_1}| = |\theta_{\alpha_2}| = 75 \pm 1$ (black lines). The red horizontal line marks the ^{8}Be energy of 3.03 MeV. Lower panel: Experimental coincidence yield for the α1-α2 particles (black points). The blue labels and arrows (3)-(8) highlight the position of known excited states of ^{8}Be as reported in Table 3, while the red label and arrow (1) indicate the central position of the 3.03 MeV level of ^{8}Be. The red points correspond to the events with $p_{\alpha_S} \leq 40$ MeV/c (see text for details).

avoid the contribution of sequential mechanism in the THM data. Only data corresponding to this range are analyzed to extract the cross section of the ^{3}He+^{5}He→2α reaction.

5 Validity test of pole approximation: The Treiman-Yang Criterion

In general, due to uncertainties that can be introduced by the presence of other mechanisms involved in the three-body reaction, in the application of IA it is important to provide some critical test of the pole approximation by a preliminary experiment. In the major part of the reactions studied through THM, these tests consisted of a comparison between the angular distribution and/or the excitation function measured with direct methods, with the ones obtained with TH reactions. The comparison takes place at low energies, but in an energy range in which significant effects due to electronic screening are not expected [49, 50].

The peculiarity of the reaction ^{5}He+^{3}He → 2α consists in the presence of an unbound particle in the input channel. This means that the tests mentioned before are not applicable since they assume direct data that are not possible to measure in this case [21].

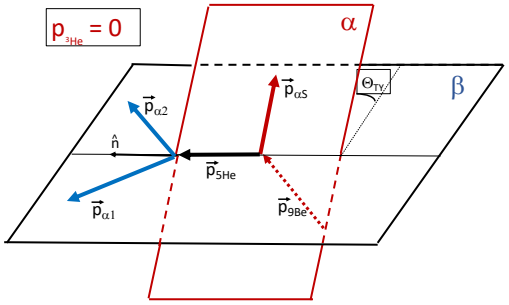

Fig. 8. Representation of the particle momenta before and after the ^{9}Be(^{3}He,$\alpha_1\alpha_2$)α_S nuclear reaction in the "anti-laboratory" system (in the $p_{^3He} = 0$ frame). Given that it proceeds through the QF reaction mechanism, θ_{TY} is the angle between the α plane and the β plane [21]

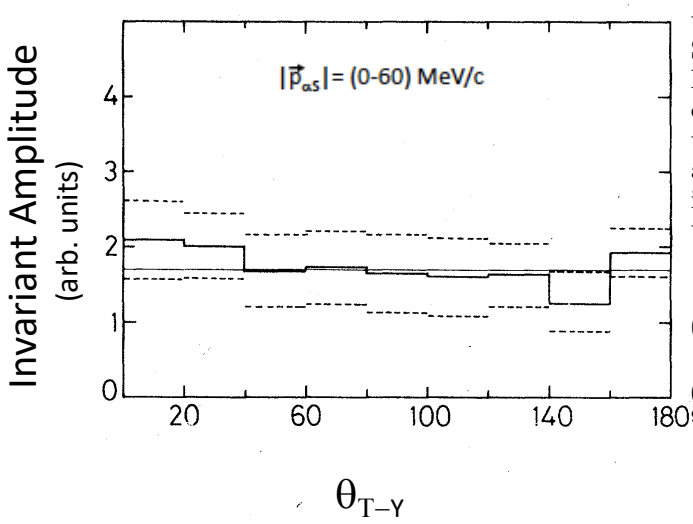

Fig. 9. Treiman-Yang angular distribution in arbitrary units (continuous lines) for the 0-60 MeV/c p_{α_S} range after subtraction of the estimated contributions from sequential mechanism. The dashed lines indicate limits considering the total uncertainties [21].

In the past, the role of the pole mechanism has been investigated in detail and attempts have been made to find sensitive criteria able to establish its relative importance. One of those criteria is the study of the distribution with respect to the Treiman-Yang angle; this criterion, first pointed out by S.B. Treiman and C.N. Yang [25], states that under given conditions such a distribution should be isotropic, confirming that the pole mechanism is dominant in the reaction.

The Treiman-Yang (T-Y) criterion is the only method for identifying the pole mechanism which is independent on the specific form of the virtual process [21,31,25]. Indeed, Eq. (1) for the pole graph represented in Fig. 1 has the remarkable characteristic that the reaction amplitude is factorized, i.e., it can be written as the product of two amplitudes and a propagator, and depends on only three variables instead of five of the general case. Hence, in the PWIA as well in the DWIA (without spin orbit dependent distortion) the three-body reaction cross section is proportional to the cross section of the virtual two-body reaction, as expressed by Eq. (1).

Inversely, according to the T-Y criterion, the reaction amplitude of the QF reaction, should be invariant under rotation by an angle θ_{T-Y}, - called T-Y angle of the plane defined by the momenta of detected particles around the sum of these momenta, in a reference frame in which either the projectile or target is at rest (anti-laboratory system) (Fig. 8) [21,25,31,35].

In the case [21], the T-Y criterion was applied to the QF contribution towards the ^{9}Be(^{3}He,$\alpha\alpha$)^{4}He reaction, in order to to study the pole approximation (factorization of the three-body cross section). The data obtained (Fig. 9) are in agreement with the prediction of the pole approximation. In particular, for an angular momentum $l = 0$ the angular distribution of T-Y is isotropic (Fig. 9) [21]. Since the validity of the pole approximation, under QF kinematic conditions, has been verified through the T-Y criterion at beam energy of 2.8 MeV (ref. [21]) lower than the one of the present work (4 MeV), we can confidently assume that the test is also usable to validate the factorization of the three-body cross section in the final state of the binary reaction ^{5}He+^{3}He → 2α.

6 Results

6.1 The excitation function of the three body ^{9}Be(^{3}He,$\alpha\alpha$)^{4}He reaction at θ_{cm}= 90°

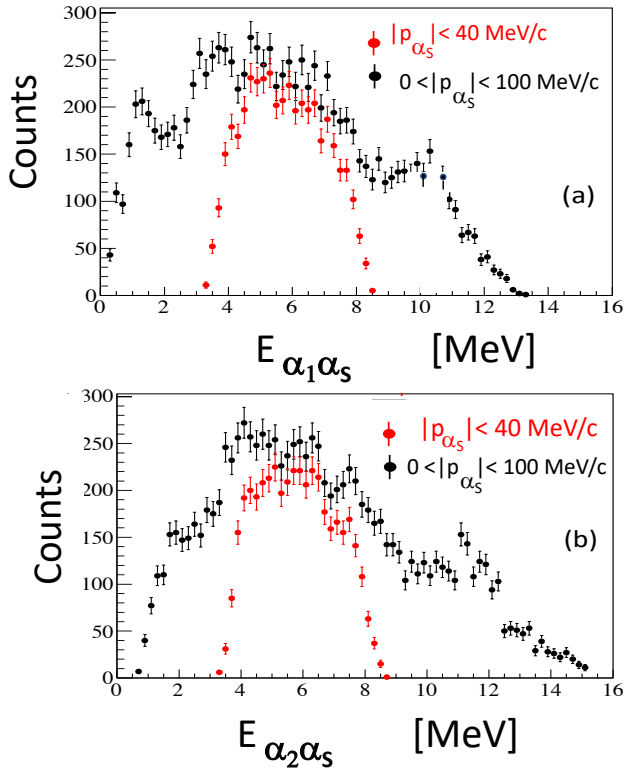

Fig. 10. Black circles represent the ^{3}He+^{9}Be coincidence yield for the angular range $67.5° \leq \theta_{\alpha_1} = |\theta_{\alpha_2}| \leq 83°$ projected on the $E_{\alpha_1\alpha_S}$ axis (a) and $E_{\alpha_2\alpha_S}$ axis (b). Red circles represent the same data selected with a cut in $p_{\alpha_S} \leq 40$ MeV/c.

The α_1-α_S (panel a) and α_2-α_S (panel b) coincidence yields of the ^{3}He+^{9}Be→ 3α reaction are shown in Fig.10 (black points). The same excitation functions corresponding to the $p_{\alpha_S} \leq 40$ MeV/c momentum range are depicted in red.

Those plots show that the selection of a restricted momentum range in the spectator particle allows us to remove the main part of the contributions by the sequential

Table 3. Resonance label and level parameters of ^{8}Be nucleus given by Tilley et al. [51]. The resonance energies E_x of the ^{8}Be states populated (in this work), spin-parities, natural widths Γ_{cm}, and observed decay channels are given.

Level n.	E_x (MeV)	J^π	Γ_{cm} (keV)	Decay channel
(1)	3.03±0.010	2^+; 0	151±15	α
(2)	11.35±0.150	4^+; 0	≈3500	α
(3)	16.626±0.003	2^+; 0+1	108±5	γ,α
(4)	16.922±0.003	2^+; 0+1	74±4	γ,α
(5)	19.235±0.010	3^+;(0)	227±16	α
(6)	19.86±0.05	4^+; 0	700±100	p,α
(7)	20.100	2^+; 0	880±20	n,p,α
(8)	20.200	0^+; 0	720±20	α
(9)	22.1±0.1	2^+;0	270±70	n,p,d,α
(10)	22.6±0.1	$(1,2)^-$;0	100±50	γ,p,α

decay via levels (1) and (2) by the correlations $\alpha_1 - \alpha_S$ and $\alpha_2 - \alpha_S$ in the analyzed data.

As mentioned before, only data reported with the red points were considered for the extraction of the ^{5}He+^{3}He→ α+α cross section. This result is in perfect agreement with previous works [19,22].

The next step of data analysis is to investigate the excitation function of the QF process in the ^{9}Be(^{3}He,$\alpha\alpha$)^{4}He reaction. Hence, the cross section measured at $p_{\alpha_S} = 0 \pm 5$ MeV/c (for α-particles emitted at 90° in the center-of-mass system) divided by the corresponding KF, was plotted as function of excitation energy of ^{8}Be (Fig. 11a), following the PWIA prescription:

$$\left[\frac{d\sigma(E_{cm},\theta_{cm}(=90°))}{d\Omega}\right]_{^3He+^5He\to 2\alpha} \propto \frac{d^3\sigma}{d\Omega_{\alpha_1} d\Omega_{\alpha_2} dE_{\alpha_1}} \cdot [KF \cdot |\phi(p_{\alpha_S}=0)|^2]^{-1} \quad (8)$$

where $|\phi(p_{\alpha_S} = 0)|^2$ is the maximum of the momentum distribution calculated for coincidence at $\theta^i_{\alpha_1}$ - $|\theta^j_{\alpha_2}|$ QF angular pairs at $E_{lab} = 4$ MeV incident energy (see Ref. [1]).

As expected, the excitation function of the QF process shows a resonant behavior peaked at ∼ 21.2 MeV of excitation energy in ^{8}Be. To cross check our result, the trend of three-body cross sections as function of energy was compared to the one present in the literature [22] [see Fig. 11(b)].

Contrary to other available data, all the points in this work were obtained from a single experiment. In the case of previous data available in the literature, the excitation function was measured through a series of experiments with beam energies between 2 and 13 MeV at symmetrical angles which should correspond to the QF contribution

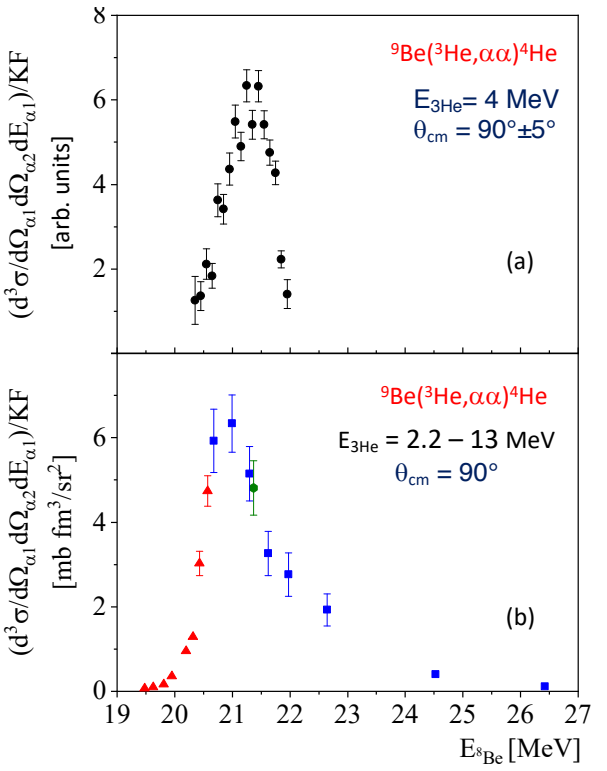

Fig. 11. Excitation function of the three-body cross section at $p_{\alpha_S} = 5 \pm 5$ MeV/c divided by kinematic factor KF: (a) present work $\theta_{cm} = 90° \pm 5°$; (b) data available in the literature for the same reaction (blue squares [22], red triangles [23], green circle [19]).

[20–24]. It is worth noticing that the two results are in good agreement, within the experimental uncertainties, despite the differences in the methods of measurement. Indeed, in the present case we have obtained comparable results using only one beam energy (4 MeV) and covering a wide angular range, thanks to the use of PSD detector, while previously the excitation functions were obtained by changing the beam energies (1.2 - 13 MeV). This is the first time that an indirect excitation function is measured through two different methods.

In addition, in the present experiment the excitation function was extracted by selecting the angular pairs at the condition $p_{\alpha S} \leq 40$ MeV/c and $\theta_{cm} = 90° \pm 5°$, while in the case of the previous the angular pairs are obtained through the condition of $|E_{cm}| \leq 0.5$ MeV [22].

6.2 Differential cross section of the ^{5}He(^{3}He,α)^{4}He virtual reaction.

Once the experimental momentum distribution $|\phi(\boldsymbol{p}_{\alpha_S})|^2$ is measured and the QF contribution data are selected, it is possible to extract the half-off-energy-shell (HOES) differential cross section.

As already mentioned, the product $(KF) \cdot |\phi(\boldsymbol{p}_{\alpha_S})|^2$ is provided by Monte Carlo simulation and following the

PWIA, the ^{3}He+^{5}He→ α+α differential cross section is given by:

$$\left(\frac{d\sigma(E)}{d\Omega}\right)^{HOES} \propto \frac{\frac{d^3\sigma}{d\Omega_{\alpha 1} d\Omega_{\alpha 2} dE_{\alpha 1}}}{KF \cdot |\phi(\boldsymbol{p}_{\alpha S})|^2_{exp}} \quad (9)$$

Again, KF takes into account masses, angles and momenta of the α_1 and α_2 particles and $|\phi(\boldsymbol{p}_{\alpha S})|^2_{exp}$ is given by the fit previously described.

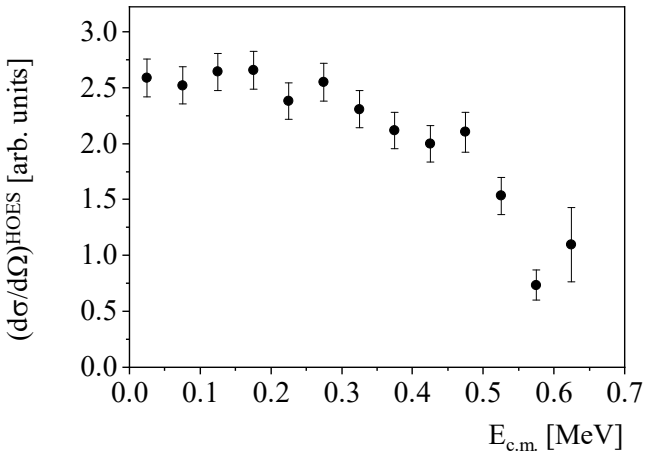

Fig. 12. Deduced HOES differential cross section of the ^{5}He+^{3}He reaction at $|\boldsymbol{p}_{\alpha_S}| \leq 40$ MeV/c in the center of mass system. The uncertainties reported in figure are only statistical.

In Fig. 12 the experimental HOES cross section is shown in the center-of-mass system in an energy range covered by the experiment. The result is reported in arbitrary units. The application of the THM assumes that the reaction is induced inside the short-range nuclear field, and the penetration probability trough the Coulomb barrier (P_l) has to be introduced to obtain the absolute value of the cross section. Indeed, the HOES differential cross section is linked to the OES one by the penetration factor of the Coulomb barrier [1,8,52] through the relation:

$$\left(\frac{d\sigma(E)}{d\Omega}\right)^{OES} \propto \left(\frac{d\sigma(E)}{d\Omega}\right)^{HOES} \cdot P_0(kr), \quad (10)$$

with $P_0(kr)$ the penetrability of the Coulomb barrier for l=0, given by

$$P_0(kr) = \frac{kr}{F_0^2(kr) + G_0^2(kr)}, \quad (11)$$

with F_0 and G_0 being regular and irregular Coulomb functions for l=0, and k and r the wave number and the interaction radius for the ^{5}He-^{3}He system, respectively, where $r = r_o([A_{^5He}]^{1/3} + [A_{^3He}]^{1/3})$ with $r_0 = 1.2$ fm

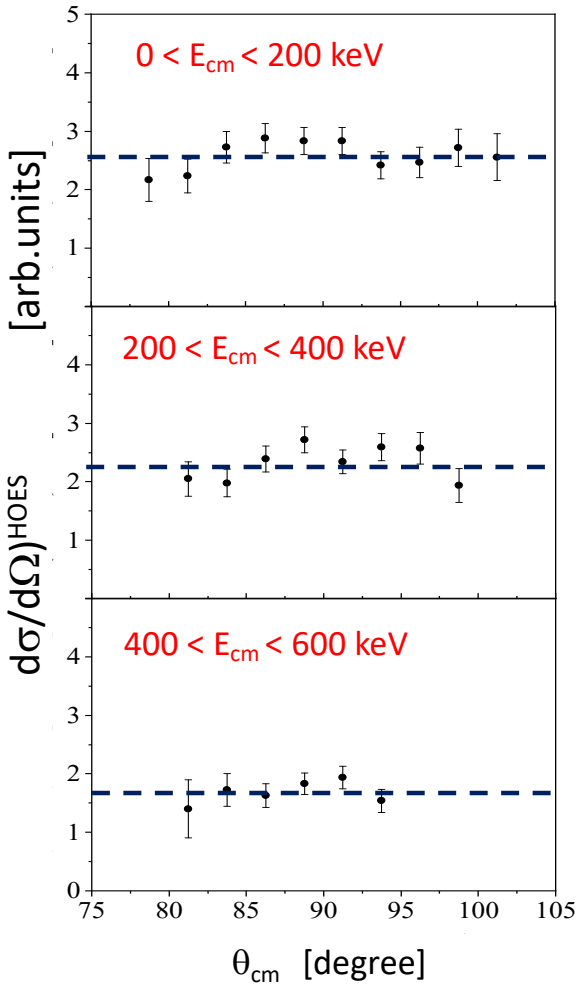

Fig. 13. Angular distributions of the TH-differential cross section in arbitrary units at different energy ranges: a) 0 keV ≤ 200 keV, b) 200 keV ≤ 400 keV and c) 400 keV ≤ 600 keV.

6.3 The angular distribution of the cross section

The penetrability factor that should be used to extract the OES cross section of interest is related to the experimental angular distribution. So, the next step of data analysis is the extraction of the angular distributions.

The relevant angle in order to get the indirect angular distribution, i.e., the emission angle for the α_1-particle in the α_1-α_2 center-of-mass system, can be calculated according to the relation [53]:

$$\theta_{c.m.} = \arccos \frac{(\boldsymbol{v}_{^3He} - \boldsymbol{v}_{^5He}) \cdot (\boldsymbol{v}_{\alpha_1} - \boldsymbol{v}_{\alpha_2})}{|\boldsymbol{v}_{^3He} - \boldsymbol{v}_{^5He}||\boldsymbol{v}_{\alpha_1} - \boldsymbol{v}_{\alpha_2}|} \quad (12)$$

where the vectors $\boldsymbol{v}_{^3He}$, $\boldsymbol{v}_{^5He}$, $\boldsymbol{v}_{\alpha_1}$, $\boldsymbol{v}_{\alpha_2}$ are the velocities of the projectile, target and of the two emitted α-particles respectively. These quantities can be calculated from their corresponding momenta in the lab system, where the momentum of the transferred particle is equal and opposite to that of the α-spectator (QF assumption) [53].

The center-of-mass angular range covered in the present experiment is $\theta_{cm} = 78° - 105°$. In Fig. 13 the experimental angular distributions are reported for different energy ranges (a) 0 keV $\leq$ 200 keV, b) 200 keV $\leq$ 400 keV and c) 400 keV $\leq$ 600 keV) spanning the full α_1 - α_2 relative energy range.

Fig. 13 clearly shows that the angular distribution for the ^{3}He(^{5}He,α)^{4}He reaction is almost isotropic in the measured angular range. In a case like this, where the $l = 0$ contribution is dominant, the differential cross section integrated over the experimental θ_{cm} range differs from the total cross section $\sigma(E)$ simply by a scaling factor (W_0) and the total cross section can be calculated as:

$$\sigma(E) = W_0 \cdot P_0(kr) \cdot [\sigma(E)]^{TH}. \quad (13)$$

The standard procedure for the TH data normalization requires an excitation function of the binary reaction of interest, in an energy region where the electron screening effect is negligible [4,41,48]. In case of the ^{5}He+^{3}He $\rightarrow 2\alpha$ reaction induced by unbound nuclei, the only data available in the literature refers to the theoretical evaluation of the differential cross section calculated via neutron transfer at $\theta_{cm} = 90°$ [19]. Since the angular distribution of the differential cross section $(\mathrm{d}\sigma/\mathrm{d}\Omega)^{HOES}$ has been shown to be constant (Fig. 13), a comparison with a small energy range is sufficient for the normalization of the TH cross section.

7 Theory

The THM can provide the excitation function of the cross section of the $^5\mathrm{He} + {}^3\mathrm{He} \rightarrow {}^4\mathrm{He} + {}^4\mathrm{He}$ reaction, but not in absolute units. Thus an appropriate scaling of the data is needed. Since there are no data available from direct experiments, only theoretical calculations can help to scale the THM data to absolute units. In this work, we use a post-form finite-range distorted-wave Born approximation to obtain the required cross section. The major steps of this approach will be presented in the following. More details can be found in Ref. [54].

The ^{5}He ground state is a resonance in the $n - {}^4$He continuum that is described as a proper scattering state. Thus the actual process in the theoretical calculation is the reaction

$$^4\mathrm{He} + n + {}^3\mathrm{He} \rightarrow {}^5\mathrm{He} + {}^3\mathrm{He} \rightarrow {}^4\mathrm{He} + {}^4\mathrm{He} \quad (14)$$

with three particles in the initial state. It is characterized by two Jacobi momenta $\boldsymbol{P}_{14}$ and $\boldsymbol{P}_{35}$, for the relative motion of the neutron with regard to ^{4}He and of the ^{3}He nucleus with regard to the ^{5}He resonant state, respectively. In the final state only the single momentum $\boldsymbol{P}_{44}$ of relative motion between the two α particles appears. Denoting with J_1, J_3, and J_4 the total angular momenta of the neutron, ^{3}He and ^{4}He, the differential transition rate of the reaction (14) is given by

$$dw = \frac{2\pi}{\hbar} \frac{1}{(2J_1+1)(2J_3+1)(2J_4+1)} \sum_{M_1 M_3 M_{4i}} \sum_{M_{4f} M'_{4f}} (15)$$
$$\int \frac{d^3P_{44}}{(2\pi\hbar)^3} \; |T_{fi}|^2 \; \delta(E_{14} + E_{35} - E_{44} + Q)$$

with the Q value

$$Q = m_4 + m_n + m_3 - m_4 - m_4 \,, \quad (16)$$

the energies $E_{ij} = P_{ij}^2/(2\mu_{ij})$ with reduced masses $\mu_{ij} = m_i m_j/(m_i + m_j)$ and the usual summation over the angular momentum projections M_1, M_3, M_{4i} in the initial state and M_{4f}, M'_{4f} in the final state. The T-matrix element T_{fi} contains all the essential information on the reaction, see below, and the δ function guarantees energy conservation. The total cross section as a function of the *cm* energy E_{35} in the ^{3}He-^{5}He system is obtained from (15), after an integration over all relative momenta $\boldsymbol{P}_{14}$ in the ^{5}He scattering continuum and momenta $\boldsymbol{P}_{44}$ in the final state as

$$\sigma(E_{35}) = \frac{\mu_{35}}{P_{35}} \int \frac{d^3P_{14}}{(2\pi\hbar)^3} \, dw \quad (17)$$
$$= \frac{\mu_{44}\mu_{35}}{(2\pi)^2\hbar^4} \frac{P_{44}}{P_{35}} \frac{1}{(2J_1+1)(2J_3+1)(2J_4+1)}$$
$$\sum_{M_1 M_3 M_{4i}} \sum_{M_4 M'_4} \int d\Omega_{44} \int \frac{d^3P_{14}}{(2\pi\hbar)^3} \, |T_{fi}|^2$$

after multiplying with the flux factor $1/v_{35} = \mu_{35}/P_{35}$ and assuming a fixed direction of $\boldsymbol{P}_{35}$.

The T-matrix element for the transition can be written in symbolic form without explicit angular momentum coupling as

$$T_{fi} = \langle \Phi_4 \Phi_{4'} \chi^{(-)}_{44'}(\boldsymbol{P}_{44}) | W | \Phi_3 \Phi^{(+)}_5(\boldsymbol{P}_{14}) \chi^{(+)}_{35}(\boldsymbol{P}_{35}) \rangle \quad (18)$$

where Φ_4, $\Phi_{4'}$, and Φ_3 are the intrinsic wave functions of the clusters ^{4}He and ^{3}He. The scattering wave functions in the initial and final state are given by distorted waves $\chi^{(+)}_{35}(\boldsymbol{P}_{35})$ and $\chi^{(-)}_{44'}(\boldsymbol{P}_{44})$, respectively, with appropriate boundary conditions. The wave function of the ^{5}He resonance is denoted by

$$\Phi^{(+)}_5(\boldsymbol{P}_{14}) = \Phi_{4'} \psi^{(+)}_{14'}(\boldsymbol{P}_{14}) \quad (19)$$

with the scattering wave function $\psi^{(+)}_{14'}$ of the neutron with respect to the ^{4}He nucleus in the initial state. The transition potential W in this approximation for T_{fi} is simply the potential U_{14} that is used to find $\psi^{(+)}_{14'}$ by solving the Schrödinger equation of relative motion. The structure of the T-matrix element (18) resembles the one that is used in the theory of the THM [6]. The main difference is, however, that a transfer reaction from the continuum to a bound state is considered here, whereas the inverse transfer reaction from a bound state to the continuum is used in the THM.

In the actual calculation of the T-matrix element, the intrinsic cluster wave function are represented by simple Gaussian wave functions

$$\Phi_3(J_3, M_3) = C_3 \exp\left[-\frac{B_3}{2}\sum_{i=1}^{3}(\boldsymbol{r}_i - \boldsymbol{R}_3)^2\right]\chi_{J_3M_3} \quad (20)$$

$$\Phi_4(J_4, M_4) = C_4 \exp\left[-\frac{B_4}{2}\sum_{i=1}^{4}(\boldsymbol{r}_i - \boldsymbol{R}_4)^2\right]\chi_{J_4M_4} \quad (21)$$

(and similarly for $\Phi_{4'}$) with normalization constants

$$C_3 = \left[\left(\frac{\pi}{B_3}\right)^3 3^{3/2}\right]^{-1/2} \quad (22)$$

and

$$C_4 = \left[\left(\frac{\pi}{B_4}\right)^{9/2} 4^{3/2}\right]^{-1/2} \quad (23)$$

and spin functions $\chi_{J_3M_3}$ and $\chi_{J_4M_4}$ of ^{3}He and ^{4}He. The vectors $\boldsymbol{R}_3 = \sum_{i=1}^{3}\boldsymbol{r}_i/3$ and $\boldsymbol{R}_4 = \sum_{i=1}^{4}\boldsymbol{r}_i/4$ are the *cm* coordinates of these nuclei and the constants $B_3 = 0.323$ fm^{-2} and $B_4 = 0.553$ fm^{-2} are determined from their point rms radii. The scattering wave functions $\chi_{35}^{(+)}(\boldsymbol{P}_{35})$, $\chi_{44}^{(-)}(\boldsymbol{P}_{44})$, and $\psi_{14'}^{(+)}(\boldsymbol{P}_{14})$ are expanded in partial waves including the full angular momentum coupling. The radial wave functions are discretized on a grid with mesh spacing 0.05 fm and obtained by solving the corresponding radial Schrödinger equations with potentials of Gaussian shape

$$V_{ij}(r_{ij}) = -V_{ij}^{(0)} \exp\left(-\frac{r_{ij}^2}{R_{ij}^2}\right) \quad (24)$$

with the two parameters depth $V_{ij}^{(0)}$ and radius R_{ij}.

For the $n - ^4$He scattering state only the $J_5^\pi = 3/2^-$ channel with orbital angular momentum $l_{14} = 0$ is considered. In order to reproduce the experimental resonance energy $E = 0.735$ MeV and width $\Gamma = 0.648$ MeV [**?**], the potential parameters are set to $V_{14}^{(0)} = 48.131$ MeV and $R_{14} = 2.449$ fm. In the final ^{4}He+^{4}He system, all partial waves with orbital angular momenta $l_{44} = 0, 2, 4, 6, 8$ are taken into account to achieve convergence. Here the potential depth and width parameter are fitted to the ^{8}Be ground state with $J^\pi = 0^+$ at 91.84 keV above the ^{4}He+^{4}He threshold and of the first excited state with $J^\pi = 2^+$ at 3.122 MeV above threshold [51]. This leads to $V_{44}^{(0)} = 50.777$ MeV and $R_{44} = 2.227$ fm. With these values the resonance widths of $\Gamma(0^+) = 4.743$ eV and $\Gamma(2^+) = 1.048$ MeV are found that are reasonably close to the experimental values of 5.57 eV and 1.513 MeV [51] given that there are only two parameters. In the ^{3}He+^{5}He scattering system the channel with $J_{35} = 0$, channel spin $S_{35} = 1$ and orbital angular momentum $l_{35} = 1$ is needed due to the constraints of angular momentum coupling. Unfortunately, there are no experimental data available to constrain the potential parameter in this channel. Since we are again in the ^{8}Be system, a transformation of the ^{4}He+^{4}He potential is used with an increased radius due to the more diffuse surface and resonance structure of the ^{3}He+^{5}He system. With a standard value of $R_{35} = 1.25$ fm $\times 8^{1/3} = 2.5$ fm one sets $V_{35}^{(0)} = V_{44}^{(0)}R_{44}^3/R_{35}^3 = 35.876$ MeV assuming identical volume integrals of the potentials. The numerical integration over all single-nucleon coordinates in (18) simplifies considerably because of the use of Gaussian potentials and wave functions of the clusters and a dependence of the transition potential W on only R_{14}, the distance between the neutron and the α particle. A two-dimensional integral in the radial coordinates R_{14} and R_{35} remains. In the integration over $\boldsymbol{P}_{14}$ in (17) energies E_{14} from 0 to 2.5 MeV are taken into account to cover the full width of the resonance. Finally, absolute values for the total cross section σ of the reaction $^5\mathrm{He} + ^3\mathrm{He} \rightarrow ^4\mathrm{He} + ^4\mathrm{He}$ are obtained. The result is depicted in Fig. 14 as a solid blue line.

7.1 Normalization of cross sections to absolute units

The unscaled cross sections of the $^5\mathrm{He} + ^3\mathrm{He} \rightarrow ^4\mathrm{He} + ^4\mathrm{He}$ reaction and uncertainties as obtained in the present THM experiment are given in arbitrary units in columns six and seven of Table 4, respectively. They are converted to actual cross sections by normalizing them in the energy range $300 - 600$ keV to the theoretical cross sections, calculated in the approach of the previous subsection. The conversion factor has the value W_0=0,87. The results are given with uncertainties in columns eight and nine of Table 4.

The scaled THM cross section is shown in Figure 14 in comparison to the theoretical values in the energy range $E_{cm} = 0 - 650$ keV in the center-of mass system. Both data set show a similar energy dependence with a slightly stronger rise of the THM data. Nevertheless, this result confirms once more the power of the THM to study nuclear reactions at very low energies inaccessible to direct experiments, in this particular case with an unstable (or unbound) nucleus in the initial state. Moreover, we would like to stress that the cross section extracted through the THM method has the advantage of not containing significant contributions from electron screening effects in the reaction ^{9}Be+^{3}He. This is due to the high beam-energy $E_{beam} = 4$ MeV compared to the beam energy (of the order of few keV) at which these effects are expected.

In the presented THM experiment, only data in a limited center-of-mass angular range were obtained. To reduce the uncertainties, a measurement covering the full 4π range is advisable, however, this will increase the required beam time substantially and call for an improved detection setup.

8 Conclusions

The results of this work clearly point out that the THM can be used to study nuclear reactions induced by an unbound nucleus x_{unb} when a suitable TH nucleus, characterized by a strong cluster configuration containing x_{unb},

Table 4. Energy in the center-of-mass system E_{cm}, event counts, statistical uncertainty, $\epsilon_{st.}$, uncertainty related to the subtraction of the background ϵ_{sf}, cross sections in arbitrary units $\sigma(E_{cm})$, total uncertainty on the cross section in arbitrary units $\Delta\sigma(E_{cm})$, cross section in absolute units $\sigma(E_{cm})$, total uncertainty in absolute units ϵ_{tot}, the relative $\frac{\Delta\sigma(E_{cm})}{\sigma(E_{cm})}$ in %.

E_{cm} [keV]	counts	$\epsilon_{st.}$ (%)	$\epsilon_{s.f.}$ (%)	ϵ_{tot} (%)	$\sigma(E_{cm})$ (arb. units)	$\Delta\sigma(E_{cm})$ (arb. units)	$\sigma(E_{cm})$ (mb)	$\Delta\sigma(E_{cm})$ (mb)	$\frac{\Delta\sigma(E_{cm})}{\sigma(E_{cm})}$ (%)
37.5	108	10.4	12.42	16.19	7.4E-9	1.1E-9	1.33E-09	0.2E-9	15
62.5	118	10.9	13.57	17.38	1.89E-6	2.82E-7	3.40E-07	0.54E-07	16
87.5	117	10.81	13.45	17.26	2.92E-5	4.34E-6	5.26E-06	0.69E-06	13
112.5	118	10.86	13.57	17.38	1.63E-4	2.42E-5	2.93E-05	0.41E-05	14
137.5	125	11.18	14.37	18.21	5.95E-4	8.74E-5	1.07E-04	0.14E-04	13
162.5	115	10.72	13.22	17.02	0.0016	2.45E-4	2.88E-04	0.43E-04	15
187.5	131	11.44	15.06	18.92	0.0046	6.82E-4	8.28E-04	1.24E-04	15
212.5	104	10.20	11.96	15.72	0.0140	0.0021	2.52E-03	0.38E-03	15
237.5	104	10.20	11.96	15.72	0.0140	0.0021	2.52E-03	0.38E-03	15
262.5	114	10.67	13.11	16.91	0.0253	0.0038	4.55E-03	0.68E-03	15
287.5	113	10.63	13.0	16.8	0.0386	0.0058	6.95E-03	1,04E-03	15
312.5	91	9.5	10.46	14.16	0.0463	0.0073	8.33E-03	1.25E-03	15
337.5	101	10	11.61	15.36	0.0730	0.0112	1.31E-02	0,20E-02	15
362.5	69	9.3	7.935	11.49	0.0683	0.0115	1.23E-02	0.21E-02	17
387.5	100	10	11.5	12.2	0.1313	0.01967	2.36E-02	0.35E-03	15
412.5	69	8.3	7.9	11.48	0.1173	0.0012	2.11E-02	0.34E-02	16
437.5	80	8.9	9.2	12.8	0.1744	0.0282	3.14E-02	0,50E-02	16
462.5	80	8.9	9.2	12.83	0.22	0.0352	3.96E-02	0.673E-02	17
487.5	61	7.8	7.02	10.50	0.21	0.36	3.78E-02	0.64E-02	17
512.5	48	6.9	5.52	8.86	0.21	0.038	3.78E-02	0.68E-02	18
537.5	36	6	4.14	7.30	0.19	0.039	3.42E-02	0.68E-02	20
562.5	15	3.9	11.61	15.36	0.073	0.003	1.31E-02	0.36E-02	28
587.5	16	4	10.46	14.16	0.050	0.003	0.9E-02	0.25E-02	28
612.5	9	3	10.35	10.78	0.16	0.040	2.88E-02	1.01E-02	35

is chosen. Here, for the first time, the ^{5}He(^{3}He,α)^{4}He nuclear reaction induced by the unbound nucleus ^{5}He, important for nuclear physics, was investigated from 650 keV down to the astrophysical region. For this purpose the THM was applied to the ^{9}Be(^{3}He,$\alpha\alpha$)^{4}He three-body QF process. The Treiman-Yang Criterion, reported in the literature and previous research [21], has supported the hypothesis of the three-body cross section factorization (at 4 MeV beam energy) [1]. After the selection of events compatible with the QF mechanism, the virtual two-body cross section has been calculated in arbitrary units at the energy range $E_{cm} = 0 - 620$ keV and angular range $78^\circ \leq \theta_{cm} \leq 115^\circ$. In addition to this experimental study, the cross section of the ^{5}He(^{3}He,α)^{4}He neutron transfer reaction was calculated employing a finite-range distorted-wave approximation with simple many-body wave functions of the clusters. The result was used to normalize the experimental data to absolute values. This will allow to consider this reaction in network calculations of big bang nucleosynthesis and r-process nucleosynthesis in a collapsar [55] which is a black-hole forming supernova and has extremely high entropy and neutron-rich conditions where the unstable nuclei like ^{5}He might play an important role.

Finally, it will be possible to study the effect of electron screening on the cross section [49,50] at the lowest energies reached, a peculiar feature of the THM. In the present THM experiment only data in a limited center-of-mass angular range were obtained.

9 Acknowledgment

C.A.B. was partially supported by the U.S. DOE Grant No. DE-FG02-08ER41533 and funding contributed by the LANL Collaborative Research Program by the Texas A&M System National Laboratory Office and Los Alamos National Laboratory. A.M.M. acknowledges support from the U.S. DOE Grant No. DE-FG02-93ER40773 and NNSA

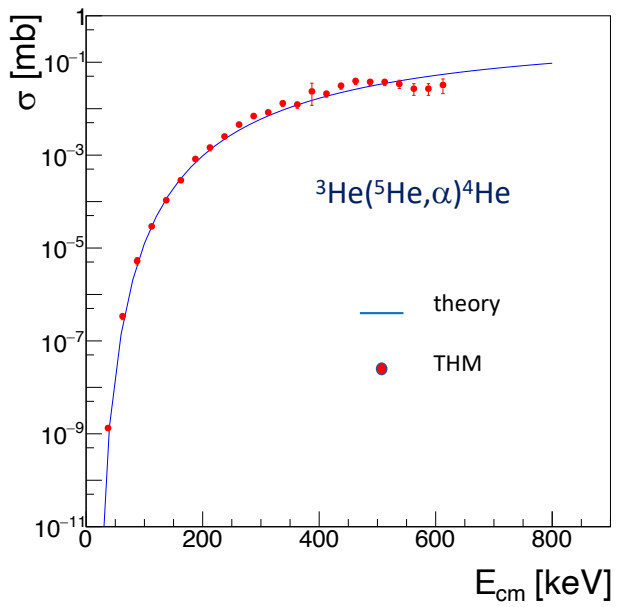

Fig. 14. Cross section of the $^5\mathrm{He} + {}^3\mathrm{He} \rightarrow {}^4\mathrm{He} + {}^4\mathrm{He}$ reaction from the THM experiment (red circles) and from theory (solid blue line).

Grant No. DENA 0003841. S.T. is grateful for the support from the LNS during a stay in January 2020 that initiated the theoretical calculation, T.K. was partially supported by Grants-in-Aid for Scientific Research of JSPS (20K03958, 17K05459). This work has been partially supported by the Italian Ministry of University (MIUR) under grant LNS - Astrofisica Nucleare (fondi premiali) and by PON RI 2014-2020 - AIM (Attraction and International Mobility), project AIM1848704-3, by the Croatian Science Foundation under project no.7194 and project n$_o$.P-2018-01-1257 and in part by the Scientific Centre of excellence for advance materials and sensor in Zagreb AIM (Attraction and International Mobility), project AIM1848704-3

References

1. C. Spitaleri, M. Lattuada, A. Cvetinović, Soić, M. Milin,P. Colović, G .D'Agata, D. Dell'Aquila, G.L. Guardo, M .Gulino, O. Trippella, M. La Cognata, L .Lamia, D. Lattuada, Li Chengbo, S .Messina, D .Nurkic, S.S. Perrotta, R.G. Pizzone, R .Popoconski, S. Romano, N. Skukan, R. Sparta, S. Szilner, M. Uroic, N. Vukman, Eur. Phys. J. A **56**, 18 (2020).
2. G. Baur, Phys. Lett. **178**, 135 (1986).
3. C. Spitaleri, in *Problems of Fundamental Modern Physics, II*: Proceedings, Ed. by R. Cherubini, P. Dalpiaz, and B. Minetti (World Sci., 1991), p. 21 (1991).
4. S. Cherubini, V.N. Kondratyev, M. Lattuada, C. Spitaleri, Đ. Miljanic, M. Zadro, and G. Baur, Astrophys. J., **457**, 855 (1996).
5. S. Typel, and H.H. Wolter, Few-Body Syst. **29**, 75 (2000).
6. S. Typel and G. Baur, Ann. of Phys. **305**, 228 (2003).
7. C. Spitaleri, S. Cherubini, A. Del Zoppo, A. Di Pietro,P. Figuera, M. Gulino, M. Lattuada, Đ. Miljanić, A. Musumarra, M.G. Pellegriti. R.G. Pizzone, C. Rolfs, S. Romano, S. Tudisco and A. Tumino, Nucl. Phys. A **719**, 99c (2003).
8. A.M. Mukhamedzhanov, L. D. Blokhintsev, B. F. Irgaziev, A. S. Kadyrov, M. La Cognata, C. Spitaleri and R. E. Tribble, J. Phys. G: Nucl. Part. Phys. **35**, 014016 (2008)
9. A.M. Mukhamedzhanov, Phys. Rev. C **84**, 044616 (2011).
10. C. Spitaleri, Proceedings of the International School of Physics "Enrico Fermi", **178**, 333-354 (2011)
11. C. Spitaleri, A.M. Mukhamedzhanov, L.D. Blokhintsev, M. La Cognata, R.G. Pizzone, and A. Tumino, Physics of Atomic Nuclei **74**, 1763 (2011).
12. R.E. Tribble, C.A. Bertulani, M. La Cognata, A.M. Mukhamedzhanov, and C. Spitaleri, Rep. Progr. Phys. **77**, 106901 (2014).
13. C. Spitaleri, M. La Cognata, L. Lamia, A.M. Mukhamedzhanov, and R.G. Pizzone, Eur. Phys. J. A **52**, 77 (2016).
14. C. Spitaleri, M. La Cognata, L. Lamia, R.G. Pizzone, A. Tumino, Euro. Phys. J. A **55**, 161 (2019).
15. S. Cherubini, M. Gulino, C. Spitaleri, G.G. Rapisarda, M. La Cognata, L. Lamia, R.G. Pizzone, S. Romano, S. Kubono, H. Yamaguchi, S. Hayakawa, Y. Wakabayashi, N. Iwasa, S. Kato, T. Komatsubara, T. Teranishi, A. Coc, N. de Sereville, F. Hammache, G. Kiss, S. Bishop, and D. N. Binh, Phys. Rev. C **92**, 015805 (2015).
16. R.G. Pizzone, B.T. Roeder, M. McCleskey, L. Trache, R.E. Tribble, C. Spitaleri, C.A. Bertulani, S. Cherubini, M. Gulino, I. Indelicato, M. La Cognata, L. Lamia, G.G. Rapisarda and R. Spartá, Eur. Phys. J. A **52**, 24 (2016).
17. Q.-G. Wen, C.-B. Li, S.-H. Zhou, B. Irgaziev, Y.-Y. Fu, C. Spitaleri, M. La Cognata, J. Zhou, Q.-Y. Meng, L. Lamia, and M. Lattuada, Phys. Rev. C **93**, 035803 (2016).
18. L. Lamia, M. Mazzocco, R.G. Pizzone, S. Hayakawa, M. La Cognata, C. Spitaleri, C.A. Bertulani, A. Boiano, C. Boiano, C. Broggini, A. Caciolli, S. Cherubini, G. D'Agata, H. da Silva, R. Depalo, F. Galtarossa, G.L. Guardo, M. Gulino, I. Indelicato, M. La Commara, G. La Rana, R. Menegazzo, J. Mrazek, A. Pakou, C. Parascandolo, D. Piatti, D. Pierroutsakou, S.M.R. Puglia, S. Romano, G.G. Rapisarda, A.M. Sánchez-Benítez, M.L. Sergi, O. Sgouros, F. Soramel, V. Soukeras, R. Spartá, E. Strano, D. Torresi, A. Tumino, H. Yamaguchi, and G. L. Zhang, Astrophys. J. **879**, 23 (2019).
19. J. Kasagi, T. Nakagawa, N. Sekine, T. Tohei, and H. Ueno, Nucl. Phys. A **239**, 233 (1975).
20. N. Arena, D. Vinciguerra, F. Riggi, and C. Spitaleri, Lettere al Nuovo Cimento **17**, 231 (1976).
21. P.G. Fallica, M. Lattuada, F. Riggi, C. Spitaleri, C.M.Sutera, and D. Vinciguerra, Phys. Rev. C **24**, 1394 (1981).
22. M. Lattuada, F. Riggi, C. Spitaleri, and D. Vinciguerra, Nucl. Phys. A **458**, 493 (1986).
23. N. Arena, D. Vinciguerra, M. Lattuada, F. Riggi, and C. Spitaleri, Il Nuovo Cimento **45**, 405 (1978).
24. S. Barbarino, M. Lattuada, F. Riggi, C. Spitaleri, and D. Vinciguerra, Phys.Rev. C **21**, 1104 (1980).
25. B. Treiman and N. Yang, Phys. Rev. Lett. **8**, 140 (1962).
26. G.R. Satchler, *Direct Nuclear Reactions*, International Series of Monographs on Physics (Oxford University Press, 1983) p. 211

27. C.A. Bertulani, *Nuclei in the Cosmos* Scientific World, (2013).
28. R.G. Pizzone, C. Spitaleri, A.M. Mukhamedzhanov, L.D. Blokhintsev, C.A. Bertulani and B.F. Irgaziev, M. La Cognata, L. Lamia, and S. Romano, Phys. Rev. C **80**, 025807 (2009).
29. R.G. Pizzone, C. Spitaleri, S. Cherubini, M. La Cognata, M. Lamia, Đ. Miljanić, A. Musumarra, S. Romano, A. Tumino, S. Tudisco, and S. Typel, Phys. Rev. C **71**, 055801 (2005).
30. G.F. Chew and G.C. Wick, Phys. Rev. **85**, 636 (1952).
31. I.S. Shapiro, Sov. Physics Uspekhi **10**, 515 (1967)
32. J.V. Meboniya, Phys Lett.A. **30**, 153 (1969).
33. N. Soic, D. Cali, S. Cherubini, E. Costanzo, M. Lattuada, M. Milin, D. Miljanić, S. Romano, C. Spitaleri, and M. Zadro, Eur. Phys. J. A **3**, 303 (1998).
34. N. Keeley, K. W. Kemper, and K. Rusek, Phys. Rev. C **64**, 031602 (2001).
35. I.S. Shapiro, Interaction of High-Energy Particles with Nuclei, International School of Physics "Enrico Fermi", Course XXXVIII, edited by E. Ericson (Academic Press, New York) p. 210 (1967).
36. E. Costanzo, M. Lattuada, S. Romano, D. Vinciguerra, and M. Zadro, Nucl. Instrum. Method in Phys. Res. A **295**, 373 (1990)
37. M. Zadro, Đ. Miljanić, C. Spitaleri, G. Calvi, M. Lattuada, and F. Riggi, Phys. Rev. C **40**, 181 (1989).
38. C. Spitaleri, M. Aliotta, S. Cherubini, M. Lattuada, Đ. Miljanić, S. Romano, N. Soić, M. Zadro, R.A. Zappala, Phys. Rev. C **60** 055802 (1999).
39. M. Lattuada, R.G. Pizzone, S. Typel, P. Figuera, Đ. Miljanić, A. Musumarra, M.G. Pellegriti, C. Rolfs, C. Spitaleri, and H.H. Wolter, Astrophys. J **562**, 1076 (2001).
40. A. Tumino, C. Spitaleri, M.L. Sergi, V. Kroha, V. Burjan, S. Cherubini, Zs. Fülöp, M. La Cognata, L. Lamia, J. Novác, R.G. Pizzone, S. Romano, E. Somorjai, S. Tudisco, and J. Vincour, Eur. Phys. J. A **27**, Supplement 243 (2006).
41. C. Spitaleri, A.M. Mukhamedzhanov, S. Typel, R.G. Pizzone, M. Aliotta, S. Blagus, M. Bogovac, S. Cherubini, P. Figuera, M. Lattuada, M. Milin, Đ. Miljanić, A. Musumarra, M.G. Pellegriti, D. Rendi'c, C. Rolfs, S. Romano, N. Soić, A. Tumino, H.H. Wolter, and M. Zadro, Phys. Rev. C **63**, 055801 (2001).
42. R.G. Pizzone, C. Spitaleri, L. Lamia, C. Bertulani, A. Mukhamedzhanov, L. Blokhintsev, V.Burjan, S. Cherubini, Z. Hons, G.G. Kiss, V. Kroha, M. La Cognata, C. Li, J. Mrazek, S. Piskor, S.M.R. Puglia, G.G. Rapisarda, S. Romano, M.L. Sergi, and A. Tumino, Phys. Rev. C **83**, 045801 (2011).
43. A. Rinollo, S. Romano, C. Spitaleri, C. Bonomo, S. Cherubini, A. Del Zoppo, P. Figuera, M. La Cognata, L. Lamia, A. Musumarra, M.G. Pellegritia, R.G. Pizzone, C. Rolf, D. Schürmann, F. Strieder, S. Tudisco and A. Tumino, Nucl. Phys. A **758**, 146c (2005).
44. A. Tumino, C. Spitaleri, A.M. Mukhamedzhanov, S. Typel, M. Aliotta, V. Burjan, M. Gimenez, M. Del Santo, G.G. Kiss, V. Kroha, Z. Hons, M. La Cognata, L. Lamia, J. Mrazek, R.G. Pizzone, S. Piskor, G.G. Rapisarda, S. Romano, M.L. Sergi, R. Spartá,, Phys. Lett. B **700**, 111 (2011).
45. R.G. Pizzone, R. Spartà, C. A. Bertulani, C. Spitaleri, M. La Cognata, J. Lalmansingh, L. Lamia, A. Mukhamedzhanov, and A. Tumino, The Astrophys. J. **786**, 112 (2014)
46. M. La Cognata, C. Spitaleri, O. Trippella, G.G. Kiss, G.V. Rogachev, A.M. Mukhamedzhanov, M. Avila, G.L.Guardo, E. Koshchiy, A. Kuchera, L. Lamia, S.M.R. Puglia, S. Romano, D. Santiago, R. Spartá, Phys. Rev. Lett. **109**, 232701 (2012).
47. G.L. Guardo, C. Spitaleri, L. Lamia, M. Gulino, M. La Cognata, X. Tang, R. de Boer, X. Fang, V. Goldberg, J. Mrazek, A. Mukhamedzhanov, M. Notani, R.G. Pizzone, G.G. Rapisarda, M.L. Sergi, and M. Wiescher, Phys. Rev. C **95**, 025807 (2017).
48. C. Spitaleri, L. Lamia, A. Tumino, R.G. Pizzone, S. Cherubini, A.Del Zoppo, P. Figuera, M.La Cognata, A. Musumarra, M.G. Pellegriti, A. Rinollo, C. Rolfs, S. Romano, and S. Tudisco, Phys. Rev. C **69**, 055806 (2004).
49. H.J. Hassenbaum, K. Lagangke, and C. Rolfs, Z.Phys. A **327**, 461 (2001).
50. F. Streider, C. Rolfs, C. Spitaleri and P. Corvisiero, Naturwissenschaften **88**, 461 (2001).
51. D.R. Tilley, J.H. Kelley, J.L. Godwin, D.J. Millener, J.E. Purcell, C.G. Sheu, and H.R. Weller, Nucl. Phys. A **745**, 155 (2004)
52. A. Tumino, C. Spitaleri, A. Mukhamedzhanov, G. G. Rapisarda, L. Campajola, S. Cherubini, V. Crucilla, Z. Elekes, Z. Fulop, L. Gialanella, M. Gulino, G. Gyorky, G. Kiss, M. La Cognata, L. Lamia, A. Ordine, R.G. Pizzone, S. Romano, M.L. Sergi, and E. Somorjai, Phys. Rev. C **78**, 064001 (2008).
53. M. Jain, P.G. Roos, H.G. Pugh, and H.D. Holmgren, Nucl. Phys. A. **153**, 49 (1970).
54. S. Typel, Eur. Phys. J. A **56**, 286 (2020).
55. M. Famiano, A.B. Balantekin, T. Kajino, M. Kusakabe, K. Mori, and Y. Luo, Astrphys. J. **898**, 163 (2020).